International Journal of Fluid Mechanics Research, Vol. 28, No. 4, 2001

# Coupled Heat and Mass Transfer by Natural Convection from a Permeable Non-Isothermal Vertical Plate Embedded in Porous Media†

**Ali J. Chamkha**
Department of Mechanical Engineering,
Kuwait University, Safat, 13060 Kuwait

Similarity equations for coupled heat and mass transfer by natural convection from a vertical semi-infinite permeable plate embedded in an isotropic porous medium in the presence of a magnetic field are developed. The developed equations allow for the presence of thermal and diffusion of species buoyancy effects, wall suction or blowing effects, as well as variable wall temperature and concentration. These general ordinary differential equations are solved numerically by an implicit finite-difference method. The obtained results are illustrated graphically for various parametric conditions to show interesting features of the solution.

* * *

## Introduction

Coupled heat and mass transfer in porous media finds application in many industrial, geothermal and geophysical engineering problems. These applications include extraction of geothermal energy, migration of moisture in fibrous insulation, the spreading of chemicals/pollutants in fibrous media, and the problem of soil contamination by crude oil as that which occurred in the State of Kuwait during the Gulf war. Despite the importance of concentration gradients in the possible suppression of convective flow induced by thermal buoyancy in such applications, coupled heat and mass transfer problems in porous media have received relatively little attention. A literature survey on this topic revealed that Trevisan and Bejan [1] considered combined heat and mass transfer by natural convection in a porous medium for various geometries. Bejan and Khair [2] reported on the natural convection boundary-layer flow in a saturated porous medium with combined heat and mass transfer. The coupled heat and mass buoyancy-induced inclined boundary layer in a porous medium was studied by Jang and Chang [3]. Later, Lai and Kulacki [4] extended the problem of Bejan and Khair [2] to include wall fluid injection effects. Early studies which considered coupled heat and mass transfer without the presence of porous media include the works of Gebhart and Pera [5] on vertical plates, Pera and Gebhart [6] and Radwan and Elbashbeshy [7] on horizontal plates, and Chen and Yuh [8] on inclined plates. Recently, Lai [9] and Yih [10] have considered coupled heat and mass transfer by mixed convection from a vertical plate embedded in a saturated

† Received 7.05.2000



ISSN 1064-2277

porous medium.

There has been increased interest in studying hydromagnetic flows of electrically conducting fluids in the presence or absence of heat generation or absorption effects due to their possible occurrence in engineering processes such as those dealing with nuclear and chemical reactors. Examples of such studies include the recent works of Vajravelu and Nayfeh [11], Chamkha [12], Vajravelu and Hadjinicolaou [13] and Elbashbeshy [14]. Motivated by the works referenced above and the possible application to the problem of soil contamination existing in Kuwait, it is of interest in this work to consider hydromagnetic natural convection flow induced by both thermal and mass diffusion effects along a vertical permeable plate embedded in a porous medium with heat generation or absorption and variable wall temperature and concentration conditions and to find the conditions for which the governing equations exhibit a self-similar solution.

## Problem Formulation

Consider steady, laminar, hydromagnetic coupled heat and mass transfer flow by natural convection along a semi-infinite vertical permeable plate embedded in a fluid-saturated porous medium. The surface of the plate is maintained at a temperature and concentration that vary as power-law functions of the distance along the plate $x$. The temperature and concentration at the plate are always greater than their uniform ambient conditions existing far from the surface. A magnetic field which varies with the distance $x$ of strength $B_0$ such that $B_0^2 = b_0 x^{-1/2}$ ($b_0$ is a constant) is applied in the y direction which is normal to the plate. A variable fluid suction or blowing is imposed at the plate surface. The fluid is assumed to be Newtonian, electrically-conducting, heat generating or absorbing and has constant properties except the density in the buoyancy term of the balance of momentum equation. The porous medium properties are assumed to vary with $x$. The magnetic Reynolds number is assumed to be small so that the induced magnetic field can be neglected. In addition, there is no applied electric field and all of the Hall effect, Joule heating, and viscous dissipation are neglected. Invoking the Boussinesq and boundary-layer approximations, the governing equations for this problem can be written as

$$\frac{\partial u}{\partial x} + \frac{\partial v}{\partial y} = 0, \tag{1}$$

$$u\frac{\partial u}{\partial x} + v\frac{\partial u}{\partial y} = \nu\frac{\partial^2 u}{\partial y^2} + \beta_T g\,(T - T_\infty) + \beta_c g\,(c - c_\infty) - \frac{\sigma B_0^2}{\rho}\,u - \frac{\nu}{K}\,u - Cu^2, \tag{2}$$

$$u\frac{\partial T}{\partial x} + v\frac{\partial T}{\partial y} = \alpha_e\frac{\partial^2 T}{\partial y^2} + \frac{Q_0}{\rho c_p}\,(T - T_\infty), \tag{3}$$

$$u\frac{\partial c}{\partial x} + v\frac{\partial c}{\partial y} = D\,\frac{\partial^2 c}{\partial y^2}, \tag{4}$$

where $u$, $v$, $T$ and $c$ are the fluid $x$-component of velocity, $y$-component of velocity, temperature and concentration, respectively; $\rho$, $\nu$, $c_p$, $\beta_T$ and $\beta_c$ are the fluid density, kinematic viscosity, specific heat at constant pressure, coefficient of thermal expansion and coefficient of concentration expansion, respectively; $\sigma$, $Q_0$ and $D$ are the fluid electrical conductivity, heat generation ($> 0$) or absorption ($< 0$) coefficient and mass diffusivity, respectively; $g$ and $B_0$ are the gravitational acceleration and magnetic induction, respectively; $K$, $C$ and $\alpha_e$ are the porous medium permeability, inertia coefficient and effective thermal diffusivity, respectively; $T_\infty$ and $c_\infty$ are the ambient fluid temperature and concentration, respectively.

The appropriate boundary conditions for this problem are

$$\begin{aligned} &u(x,0)=0, \qquad v(x,0)=-v_0(x), \qquad T(x,0)=T_w=\lambda x^m+T_\infty, \\ &c(x,0)=c_w=\gamma x^n+c_\infty, \qquad u(x,\infty)=0, \qquad T(x,\infty)=T_\infty, \qquad c(x,\infty)=c_\infty, \end{aligned} \tag{5}$$

where $v_0(x)$ is the suction velocity and $\lambda$, $\gamma$, $m$ and $n$ are all constants. By introducing the stream function $\psi$ such that $u=\partial\psi/\partial y$ and $v=-\partial\psi/\partial x$, it is convenient to nondimensionalize the above equations by using

$$\begin{aligned} x=LX, \qquad y=\frac{LY}{\mathrm{Gr}^{1/4}}, \qquad \Psi=\frac{\psi\mathrm{Gr}^{1/4}}{UL}, \qquad \theta=\frac{T-T_\infty}{T_w-T_\infty}, \qquad \phi=\frac{c-c_\infty}{c_w-c_\infty}, \\ \mathrm{Gr}=\frac{g\beta_T L^3(T_w-T_\infty)}{\nu^2}, \qquad U=\sqrt{g\beta_T L(T_w-T_\infty)}, \end{aligned} \tag{6}$$

where $L$ is a characteristic plate length, to yield

$$\frac{\partial\Psi}{\partial Y}\frac{\partial^2\Psi}{\partial X\partial Y}-\frac{\partial\Psi}{\partial X}\frac{\partial^2\Psi}{\partial Y^2}=\frac{\partial^3\Psi}{\partial Y^3}+\theta+e\phi-(M+A)\frac{\partial\Psi}{\partial Y}-B\left(\frac{\partial\Psi}{\partial Y}\right)^2, \tag{7}$$

$$\frac{\partial\Psi}{\partial Y}\frac{\partial\theta}{\partial X}+\frac{m}{X}\frac{\partial\Psi}{\partial Y}\theta-\frac{\partial\Psi}{\partial X}\frac{\partial\theta}{\partial Y}=\frac{1}{\mathrm{Pr}}\frac{\partial^2\theta}{\partial Y^2}+\delta\theta, \tag{8}$$

$$\frac{\partial\Psi}{\partial Y}\frac{\partial\phi}{\partial X}+\frac{n}{X}\frac{\partial\Psi}{\partial Y}\phi-\frac{\partial\Psi}{\partial X}\frac{\partial\phi}{\partial Y}=\frac{1}{\mathrm{Sc}}\frac{\partial^2\phi}{\partial Y^2}, \tag{9}$$

where

$$\begin{aligned} e=\frac{\beta_c(c_w-c_\infty)}{\beta_T(T_w-T_\infty)}, \qquad M=\frac{\sigma B_0^2 L}{\rho U}, \qquad A=\frac{\nu L}{KU}, \\ B=CL, \qquad \mathrm{Pr}=\frac{\nu}{\alpha_e}, \qquad \delta=\frac{LQ_0}{\rho c_p U}, \qquad \mathrm{Sc}=\frac{\nu}{D} \end{aligned} \tag{10}$$

are the buoyancy ratio coefficient, square of the Hartmann number, inverse Darcy number, dimensionless porous medium inertia coefficient, effective Prandtl number, dimensionless heat generation or absorption coefficient and Schmidt number, respectively.

Invoking the transformation

$$\eta=\frac{Y}{X^{1/4}}, \qquad \Psi=X^{3/4}f(\eta) \tag{11}$$

yields the following similar equations

$$f'''+\frac{3}{4}ff''-\left(\frac{1}{2}+B\right)f'^2-(M+A)f'+\theta+e\phi=0, \tag{12}$$

$$\frac{\theta''}{\mathrm{Pr}}+\frac{3}{4}f\theta'-m\theta f'+\delta\theta=0, \tag{13}$$

$$\frac{\theta''}{\mathrm{Sc}}+\frac{3}{4}f\phi'-n\phi f'=0, \tag{14}$$

(where a prime denotes ordinary differentiation with respect to $\eta$) provided that the applied magnetic field, the permeability and inertia of the porous medium and the heat generation or absorption coefficient must vary along the plate. Specifically, the variations with respect to the distance along the plate $x$ is such that $B_0^2(X)\alpha X^{-1/2}$, $K(X)\alpha X^{1/2}$, $C(X)\alpha X^{-1}$ and $\delta(X)\alpha X^{-1/2}$. Although,

this situation may find some applications in certain processes, such as filtration, these assumptions present a limitation to the similar equations. Another way to think of these equations is that they are locally similar since some of the parameters are still functions of $X$. The transformed boundary conditions become

$$\begin{aligned} f'(0) = 0, \qquad f(0) = f_0, \qquad \theta(0) = 1, \qquad \phi(0) = 1, \\ f'(\infty) = 0, \qquad \theta(\infty) = 0, \qquad \phi(\infty) = 0, \end{aligned} \tag{15}$$

where $f_0 = 4v_0 \mathrm{Gr}^{1/4}/3UX^{-1/4}$ is the dimensionless wall mass transfer such that $f_0 > 0$ indicates suction and $f_0 < 0$ indicates blowing or injection at the plate surface.

Of special interest for this flow and heat transfer situation are the skin-friction coefficient, Nusselt number, and the Sherwood number. These are defined in dimensionless form (see Elbashbeshy [14]) as

$$C_f = f''(0), \qquad \mathrm{Nu} = -\theta'(0), \qquad \mathrm{Sh} = -\phi'(0). \tag{16}$$

## Numerical Method

Equations (12) through (14) are nonlinear and must be solved numerically with iteration subject to the boundary conditions given in Eqs. (15). The implicit finite-difference method discussed by Blottner [15] has proven to be accurate for the solution of such equations. The method starts with a change in variable ($V = f'$) in order to reduce Eq. (12) into a second-order differential equation. Then, this equation along with Eqs. (13) and (14) will have the general form

$$\pi_1 F'' + \pi_2 F' + \pi_3 F + \pi_4 = 0, \tag{17}$$

where $F$ is a typical dependent variable and the $\pi$'s are functions of the dependent (and independent if present) variables.

At the $i$-th stage of the iteration process, linear equations are created by evaluating the dependent variables appearing in the $\pi$'s in Eq. (17) using the last value produced by the iteration process. These equations are then discretized using three-point central-difference quotients to give a set of linear algebraic equations for each dependent variable of the form

$$A_n (F_i)_{n-1} + B_n (F_i)_n + C_n (F_i)_{n+1} = D_n, \tag{18}$$

where $A_n$, $B_n$, $C_n$ and $D_n$ are functions of the $\pi$'s and the step sizes used in the $\eta$ direction. The subscripts $i$ and $n$ denote the $i$-th iteration and the $n$-th point along the $\eta$ direction, respectively.

Eq. (18) represents a tri-diagonal set of $N-2$ linear algebraic equations which are solved by the well known Thomas' algorithm or Potters method as discussed by Carnahan et al. [16] and Blottner [15]. After many numerical experiments performed to assess grid independence, it was decided to use a constant step size of 0.01. This value was shown to be adequate for obtaining accurate and grid-independent solutions. The convergence criterion for this problem required that the difference between the current and the previous iterations be $10^{-5}$. Once the solutions for $V$, $\theta$ and $\phi$ are converged, the equation $V = f'$ is solved for $f(\eta)$ by the trapezoidal rule.

Many results were obtained throughout the course of this work. A representative set is presented in Fig. 1 through Fig. 12 and Table 1 through Table 6 to show the influence of the physical parameters on the solutions.

It should be mentioned here that although Elbashbeshy [14] has used the same similarity transformations, he obtained slightly different equations in which the $1/2$ and $3/4$ factors are missing. In addition, the solution to his equations appears to be inaccurate since his solutions for $f'$, $\theta$ and $\phi$ do not asymptotically approach the ambient values as they should. Therefore, the wall slopes for velocity, temperature, and concentration are inaccurate. These facts hindered the comparison process with the results of Elbashbeshy [14]. However, the finite-difference numerical solutions of Eqs. (12) through (15) to be reported subsequently were checked and validated by separate numerical solutions using the fourth-order Runge-Kutta method. This lends confidence to the numerical results to be reported next.

## Results and Discussion

Figs. 1 and 2 present typical velocity and temperature profiles for various values of the inverse Darcy number $A$, respectively. Physically speaking, the presence of a porous medium adjacent to the vertical plate presents resistance to flow. This resistance tends to increase as the porous medium becomes more tight, i. e. as the inverse Darcy number increases. This reduction in flow velocity is accompanied by slight increases in the fluid temperature. The condition for which $A = 0$ (and $B = 0$) represents the case of no porous medium present. In these two figures, when $A$ is set to zero, $B$ was also set to zero in order to represent that condition. The physical behaviours of $f'$ and $\theta$ are depicted in the decreases of $f'$ and increases in $\theta$ as $A$ increases as shown in Fig. 1 and Fig. 2. It should be noted that in order to minimize the number of graphs to be presented, the Schmidt number Sc was set equal to the Prandtl number Pr and the heat generation or absorption coefficient $\delta$ was set to zero. In this case, the concentration profiles will look exactly the same as the temperature profiles since they are governed by similar equations and boundary conditions. Therefore, increases in $A$ will also produce increases in the concentration $\phi$.

Fig. 3 and Fig. 4 illustrate the influence of wall suction or injection on the velocity and temperature profiles, respectively. Imposition of fluid suction at the plate surface ($f_0 > 0$) have the tendency to reduce the thickness of the boundary layer present close to the wall. Thus, causing the velocity, temperature and concentration profiles to decrease at every point far from the plate. On the other hand, blowing or injection of fluid at the surface will produce the opposite effect in which the boundary layer thickness becomes thicker and the velocity and temperature as well as the concentration of the fluid increase. These behaviours are clear from Fig. 3 and Fig. 4, respectively.

The influence of the wall temperature power index $m$ on the profiles of $f'$ and $\theta$ is displayed in Fig. 5 and Fig. 6, respectively. From Eq. (13) one can observe that increases in the parameter m cause reductions in the temperature profiles $\theta$. Therefore, through the coupling between the velocity field and the temperature field by thermal buoyancy, the velocity profiles also decrease. These behaviours are clear from Fig. 5 and Fig. 6.

The effect of the ratio of concentration buoyancy to the thermal buoyancy $e$ on the velocity and temperature profiles are displayed in Fig. 7 and Fig. 8, respectively. The condition for which $e = 0$ corresponds to the absence of concentration buoyancy effects. Obviously, the presence of these effects enhances the total buoyancy influences, thus, causing higher fluid flow along the vertical plate at the expense of fluid temperature and concentration. This is depicted in the increases in $f'$ and decreases in $\theta$ (and $\phi$) shown in Fig. 7 and Fig. 8.

Fig. 9 and Fig. 10 present representative velocity and temperature profiles for various values of the square of the Hartmann number M, respectively. It is a known fact that application of a transverse magnetic field normal to the flow direction results in a flow-resistive force called the Lorentz force in the opposite direction of flow. Similar to the presence of the porous medium, this force has the

effect of slowing the motion of the fluid and increasing its temperature and concentration. These behaviours are clearly shown in Fig. 9 and Fig. 10.

Fig. 11 presents the influence of the heat generation or absorption coefficient $\delta$ on the temperature profiles. It is clear from this figure that increasing $\delta$ causes increases in the profiles of $\theta$. In addition, for heat absorption conditions ($\delta < 0$) the thermal boundary-layer thicknesses is predicted to be less than that of the case ($\delta = 0$) (thermally neutral case).

Fig. 12 depicts the effects of Schmidt's number on the concentration ($\phi$) profiles. Similar to the effect of Pr on $\theta$, increasing Sc causes the concentration of the fluid as well as the concentration boundary layer to decrease as is evident from the figure. It should be mentioned that, for the parametric conditions used to obtain these figures, higher values of Sc caused part of the concentration profile to become negative. For this reason, only Sc $= 0.7, 0.8, 0.9$ and $1.0$ are shown in Fig. 12.

Table 1 presents representative values for the skin-friction coefficient $C_f$, the Nusselt number Nu and the Sherwood number Sh for various values of the square of the Hartmann number M, respectively. Inspection of Fig. 9 and Fig. 10 shows that as M increases, the wall slopes of the velocity and temperature profiles decrease and increase, respectively, causing the values of $C_f$ and Nu to decrease (see Eq. (16)). For the same reason, the values of Sh decrease with increasing magnetic field strength. It is obvious that the effects of $A$ and $B$ on $C_f$, Nu and Sh are the same as M since all of them represent flow-resistance mechanisms. For this reason, no results will be shown for $A$ and $B$.

Table 2 depicts the influence of wall suction or injection on the values of $C_f$, Nu, and Sh, respectively. Again, Fig. 3 shows that the slope of the velocity profiles at the plate surface ($\eta = 0$) decreases as the suction velocity $f_0$ increases. This results in reductions in the values of $C_f$. On the other hand, increasing the value of $f_0$ has a tendency to increase the values of both Nu and Sh as is evident from Table 2.

Table 3 illustrates the variations in the values of $C_f$, Nu and Sh as a result of changing the ratio of concentration to thermal buoyancy effects $e$. As mentioned before, increases in the values of $e$ tend to increase the fluid flow along the plate with increasing wall velocity slopes. This produces increases in the wall friction coefficient $C_f$. Increases in e have a similar effect on the Nu and Sh as that produced by increasing $f_0$, namely, an increase in the values of both Nu and Sh. These behaviours are clearly shown in Table 3.

The influence of increasing the wall temperature power index $m$ on the values of $C_f$, Nu and Sh is displayed in Table 4. Obviously, increasing the value ofm causes reductions in the fluid temperature field and increases in the values of Nu. This causes lower thermal buoyancy effects, flow velocities, and wall friction effects. However, Table 4 shows that while Nu increases as m increases, the values of Sh tend to decrease. The opposite was predicted when the wall concentration power index $n$ was increased, namely a decrease in the values of $C_f$ and Nu and an increase in the values of Sh.

Table 5 elucidates the features of $C_f$, Nu and Sh as a result of altering the heat generation or absorption coefficient $\delta$. The increase in the temperature field as the value of $\delta$ increases enhances the thermal buoyancy-induced flow. This causes the wall slope of the fluid velocity and, therefore, $C_f$ to increase. The same is predicted for the values of Sh. On the other hand, the values of Nu show a decreasing trend with increases in the values of $\delta$.

Finally, Table 6 shows that the values of both $C_f$ and Sh decrease while the values of Nu increase due to increases in the values of the effective Prandtl number Pr. It should be mentioned that the opposite effect, namely reductions in $C_f$ and Nu and increases in Sh, was found when the Schmidt number Sc was increased.

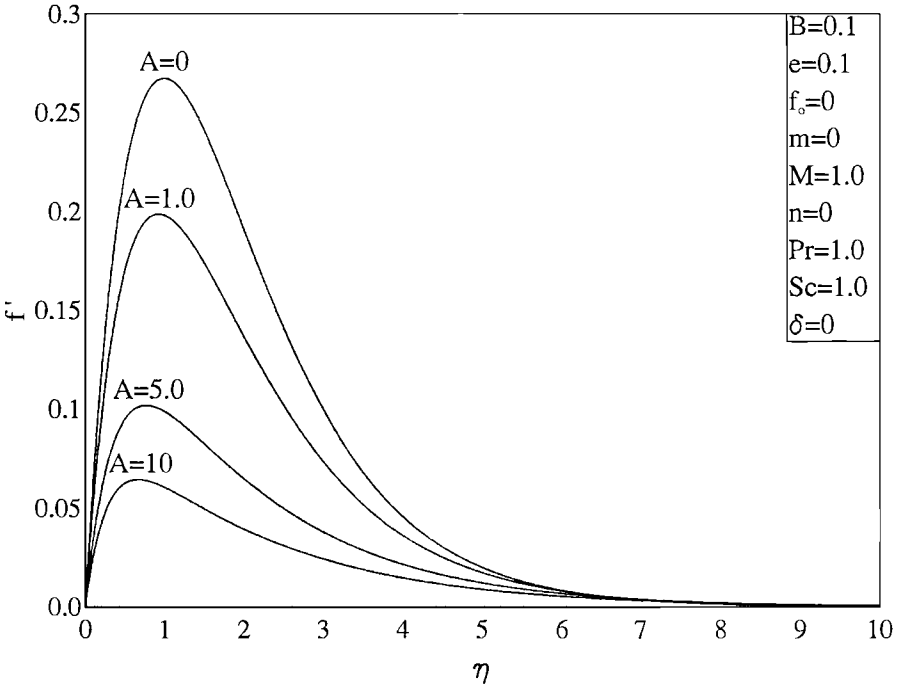


**Fig. 1.** Effects of $A$ on velocity profiles.

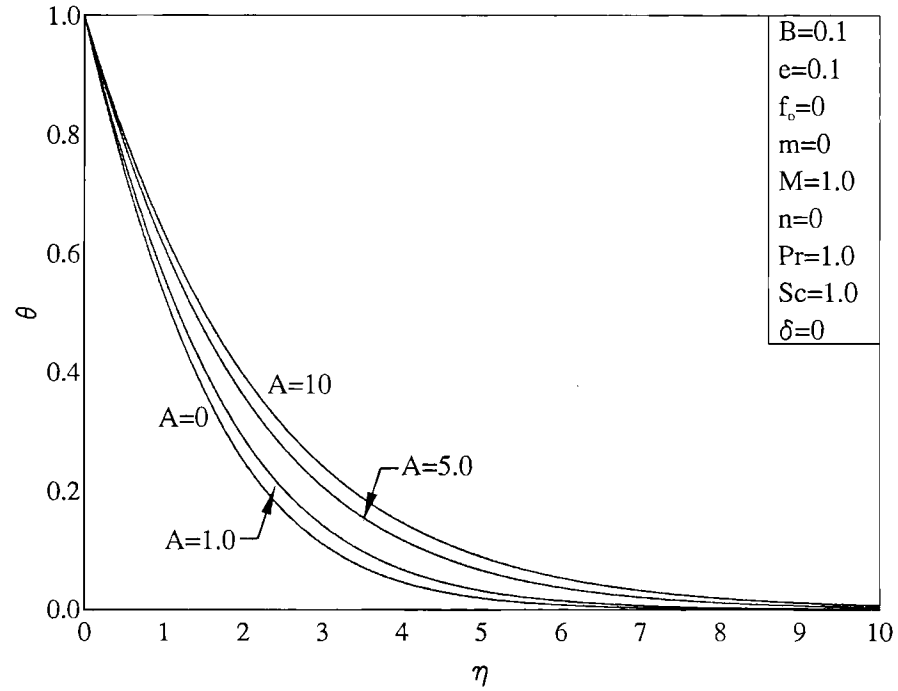


**Fig. 2.** Effects of $A$ on temperature profiles.

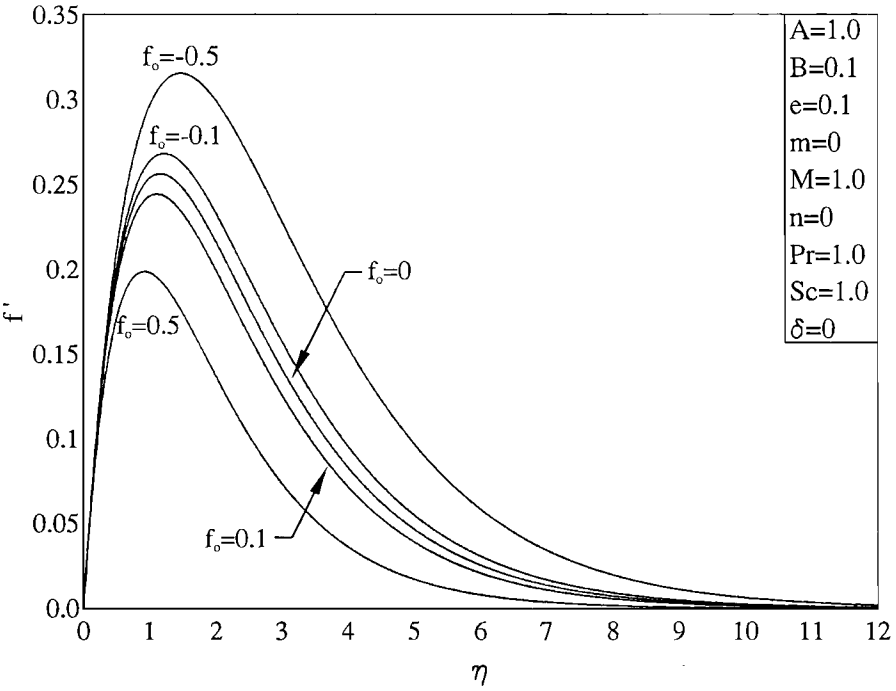


**Fig. 3.** Effects of $f_0$ on velocity profiles.

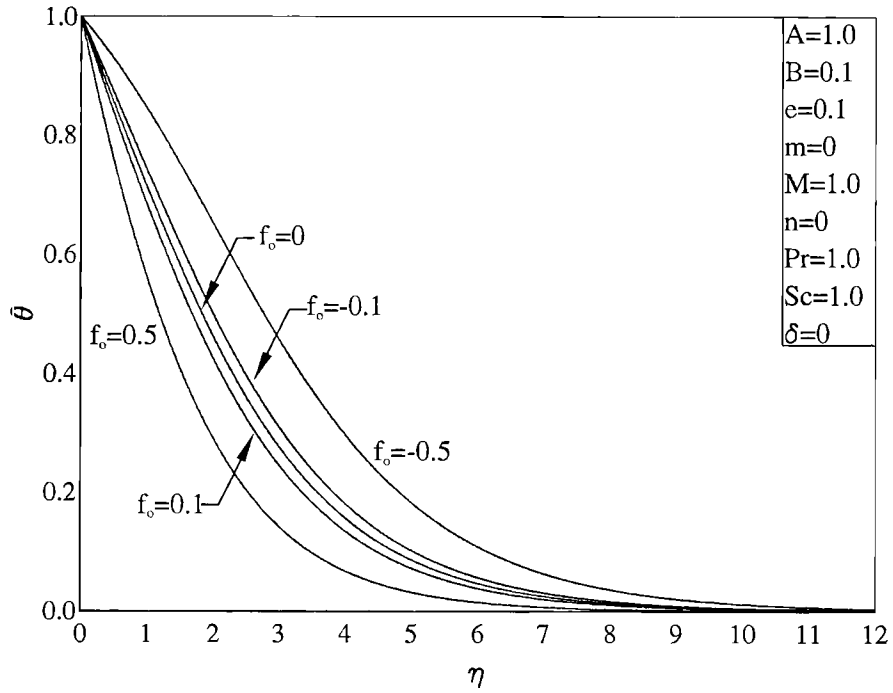


**Fig. 4.** Effects of $f_0$ on temperature profiles.

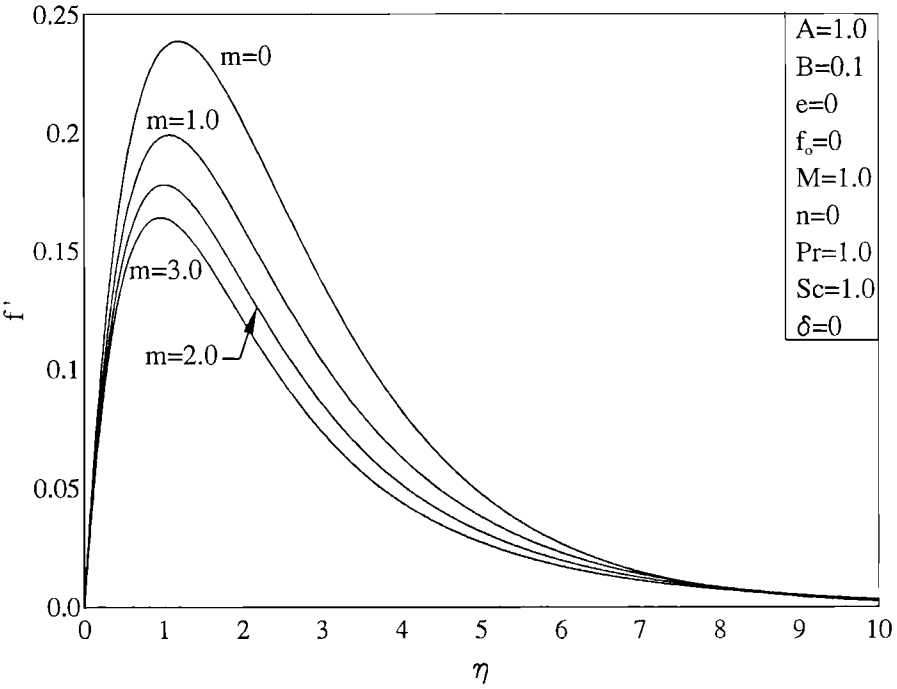


**Fig. 5.** Effects of $m$ on velocity profiles.

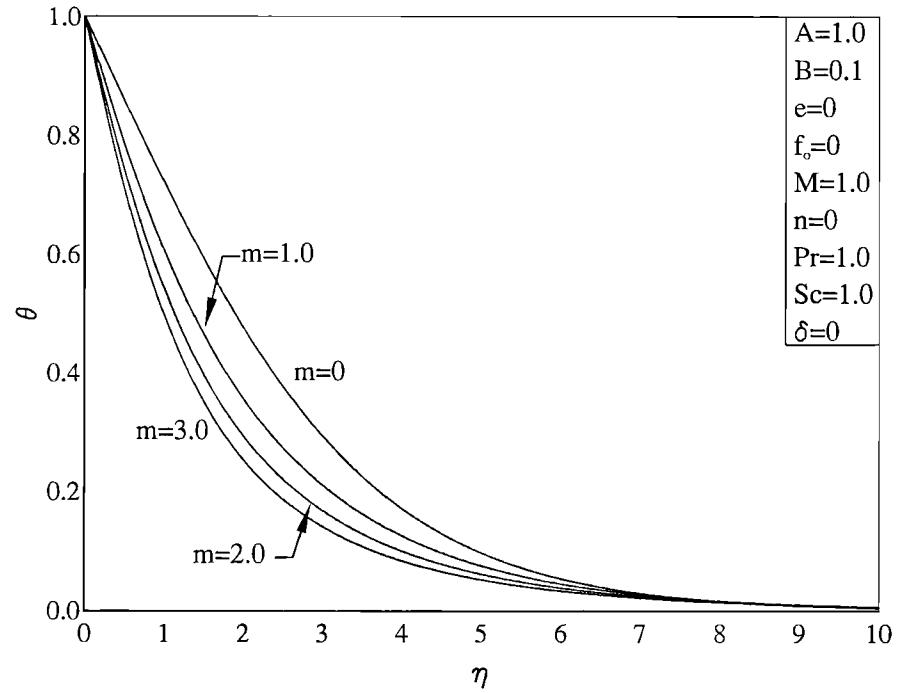


**Fig. 6.** Effects of $m$ on temperature profiles.

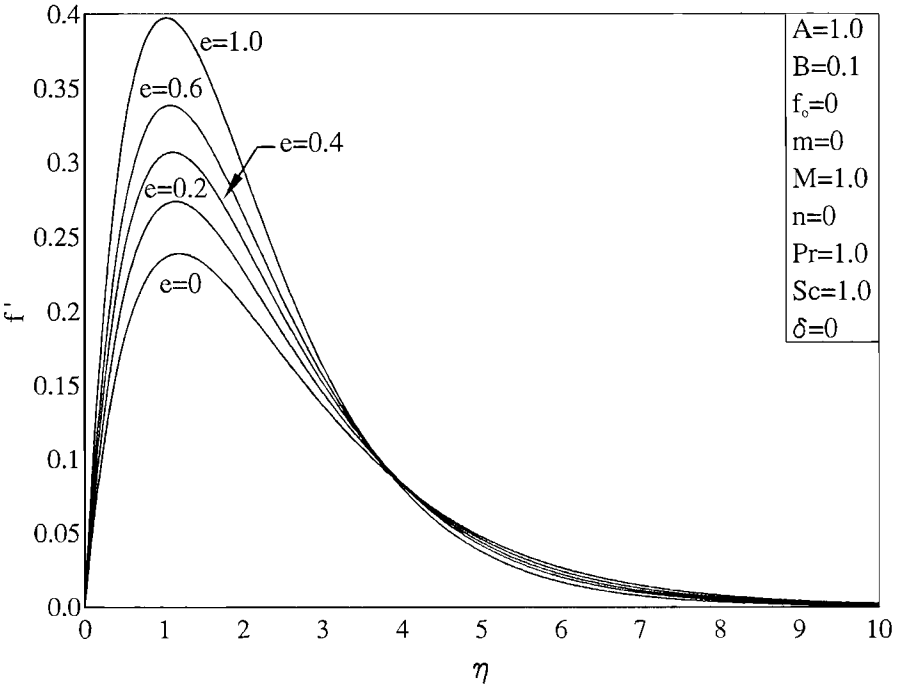


**Fig. 7.** Effects of $e$ on velocity profiles.

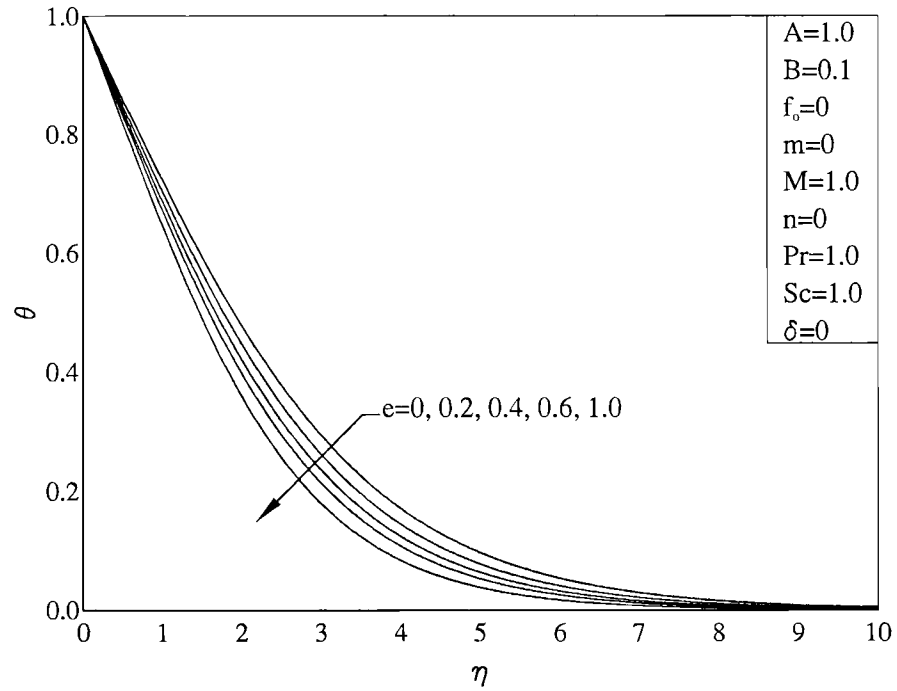


**Fig. 8.** Effects of $e$ on temperature profiles.

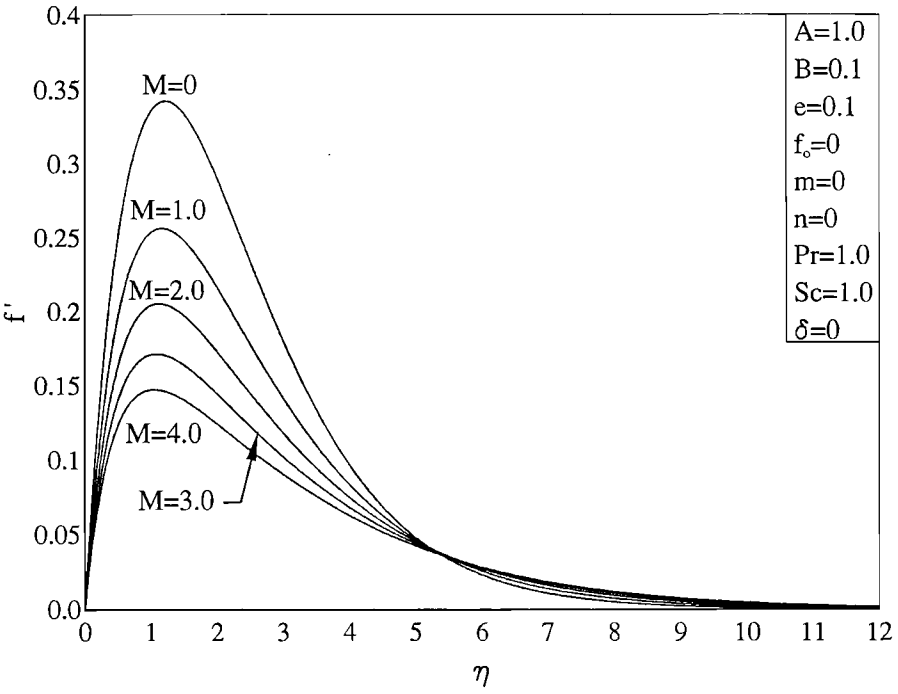


**Fig. 9.** Effects of M on velocity profiles.

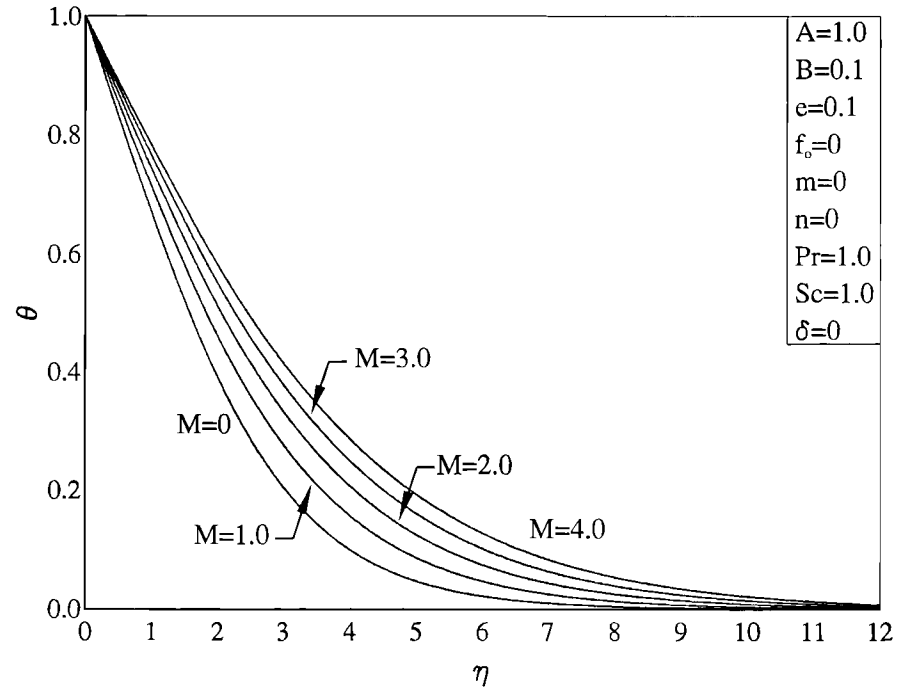


**Fig. 10.** Effects of M on temperature profiles.

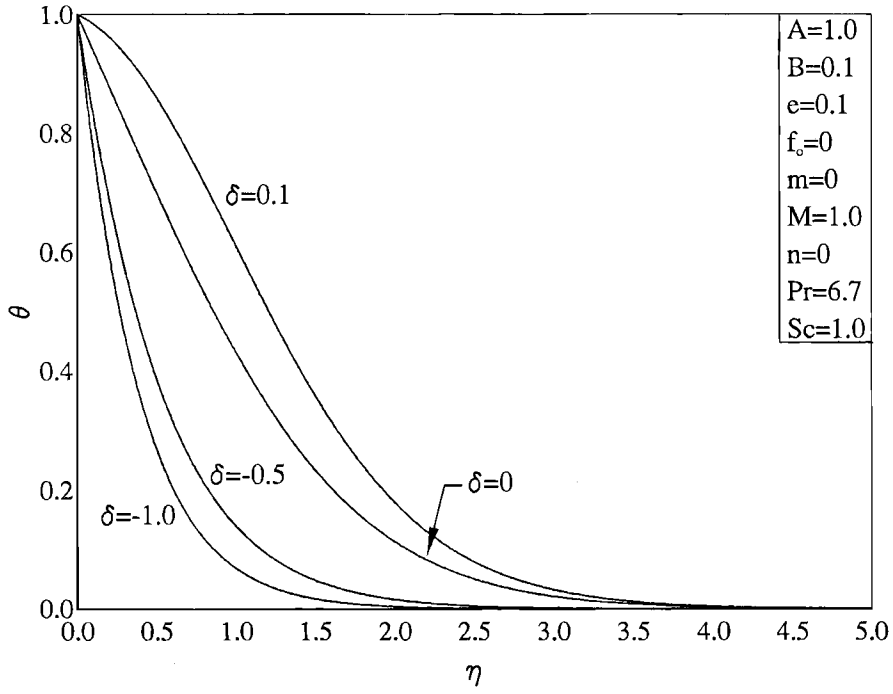


**Fig. 11.** Effects of $\delta$ on temperature profiles.

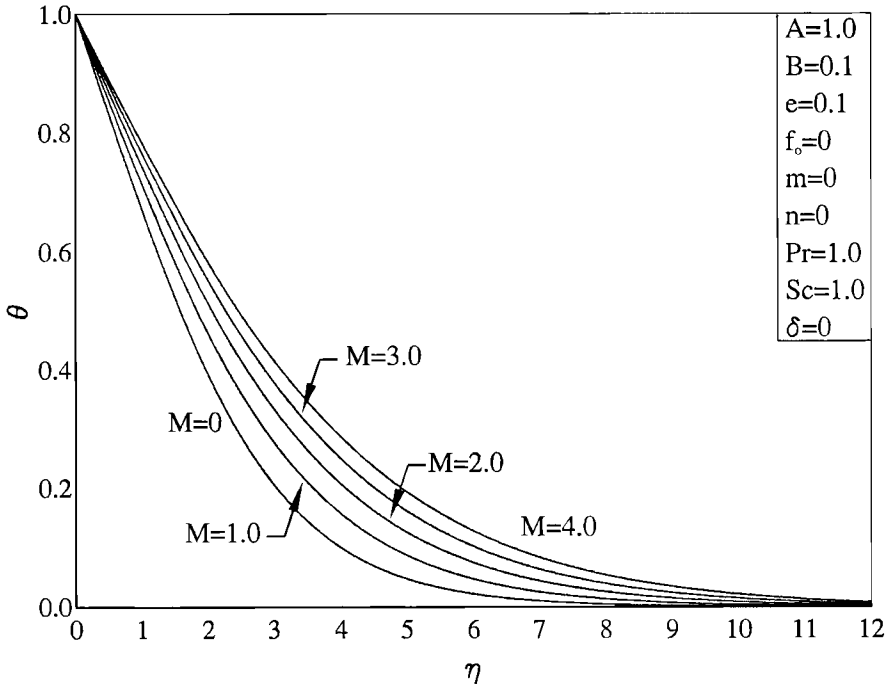


**Fig. 12.** Effects of Sc on concentration profiles.

Table 1
Effects of M on $C_f$, Nu and Sh
($A = 1.0$, $B = 0.1$, $e = 0.1$, $f_0 = 0$, $m = 0$, $n = 0$, Pr $= 1.0$, Sc $= 0.8$, $\delta = 0$)

Table 2
Effects of $f_0$ on $C_f$, Nu and Sh
($A = 1.0$, $B = 0.1$, $e = 0.1$, $m = 0$, M $= 1.0$, $n = 0$, Pr $= 1.0$, Sc $= 0.8$, $\delta = 0$)

| M | Cf | Nu | Sh |
|---|---|---|---|
| 0 | 0.73580 | 0.33744 | 0.28338 |
| 1 | 0.61409 | 0.29207 | 0.24716 |
| 2 | 0.53708 | 0.26092 | 0.22222 |
| 3 | 0.48300 | 0.23793 | 0.20383 |
| 4 | 0.44240 | 0.22015 | 0.18957 |

| $f_0$ | $C_f$ | Nu | Sh |
|---|---|---|---|
| -0.5 | 0.60273 | 0.13130 | 0.11596 |
| -0.1 | 0.61410 | 0.25391 | 0.21412 |
| 0 | 0.61395 | 0.29310 | 0.24527 |
| 0.1 | 0.61270 | 0.33516 | 0.27906 |
| 0.5 | 0.59672 | 0.53426 | 0.43840 |

Table 3
Effects of $e$ on $C_f$, Nu and Sh
($A = 1.0$, $B = 0.1$, $f_0 = 0$, $m = 0$, M $= 1.0$, $n = 0$, Pr $= 1.0$, Sc $= 0.8$, $\delta = 0$)

Table 4
Effects of $m$ on $C_f$, Nu and Sh
($A = 1.0$, $B = 0.1$, $f_0 = 0$, M $= 1.0$, $n = 0$, Pr $= 1.0$, Sc $= 1.0$, $\delta = 0$)

| $e$ | $C_f$ | Nu | Sh |
|---|---|---|---|
| 0 | 0.56226 | 0.28033 | 0.23772 |
| 0.2 | 0.66536 | 0.30318 | 0.25601 |
| 0.4 | 0.76654 | 0.32336 | 0.27221 |
| 0.6 | 0.86601 | 0.34162 | 0.28679 |
| 1.0 | 1.06053 | 0.37355 | 0.31230 |

| $m$ | $C_f$ | Nu | Sh |
|---|---|---|---|
| 0 | 0.56227 | 0.28051 | 0.28051 |
| 1 | 0.51634 | 0.44048 | 0.20222 |
| 2 | 0.48996 | 0.53951 | 0.16657 |
| 3 | 0.47152 | 0.61300 | 0.14553 |

Table 5
Effects of $\delta$ on $C_f$, Nu and Sh
($A = 1.0$, $B = 0.1$, $e = 0.1$, $f_0 = 0$, $m = 0$, M $= 1.0$, $n = 0$, Pr $= 6.7$, Sc $= 1.0$, $\delta = 0$)

Table 6
Effects of Pr on $C_f$, Nu and Sh
($A = 1.0$, $B = 0.1$, $e = 0$, $f_0 = 0$, $m = 0$, M $= 1.0$, $n = 0$, Sc $= 1.0$, $\delta = 0$)

| $\delta$ | $C_f$ | Nu | Sh |
|---|---|---|---|
| 1 | 0.31285 | 2.60510 | 0.06690 |
| 0.5 | 0.36464 | 1.86491 | 0.07707 |
| 0 | 0.50896 | 0.60997 | 0.13741 |
| 0.1 | 0.58399 | 0.12356 | 0.19012 |

| Pr | $C_f$ | Nu | Sh |
|---|---|---|---|
| 1 | 0.61720 | 0.29602 | 0.13590 |
| 6.7 | 0.51005 | 0.61130 | 0.09167 |
| 10 | 0.48450 | 0.70284 | 0.08638 |

## Conclusion

The problem of coupled heat and mass transfer by natural convection from a semi-infinite, permeable, vertical flat plate at arbitrary temperature and concentration embedded in a porous medium and in the presence of a magnetic field and heat generation or absorption effects has been examined. The conditions for obtaining similarity equations are identified. The similarity equations are solved numerically by an accurate, implicit, iterative, finite-difference method. Graphical results for the velocity and temperature profiles and tabulated results for the skin-friction coefficient, Nusselt number, and the Sherwood number have been presented for various parametric conditions. It was found that the skin-friction coefficient decreased as either of the magnetic field strength, suction velocity, wall temperature power index, wall concentration power index, effective Prandtl number, or the Schmidt number was increased. However, the skin-friction coefficient increased as either of the ratio of concentration buoyancy to thermal buoyancy coefficient or the heat generation coefficient was increased. In addition, reductions in the values of both, the Nusselt number and the Sherwood number were predicted as either of the magnetic field strength or the porous medium inverse Darcy number increased. Increases in their values were observed as either of the suction velocity or the coefficient of concentration to thermal buoyancies increased. Also, the Nusselt number increased and the Sherwood number decreased as either of the effective Prandtl number or the wall temperature power index was increased. However, the reverse effect was obtained as either of the Schmidt number or the wall concentration power index was increased. Finally, increasing the heat generation coefficient produced significant reductions in the Nusselt number and slight increases in the Sherwood number.

## REFERENCES


1. Trevisan, O. V. and Bejan, A., *Adv. Heat Transfer*, 1990, **20**, 315.
2. Bejan, A. and Khair, K. R., *Int. J. Heat Mass Transfer*, 1985, **28**, 909.
3. Jang, J. Y and Chang, W. J., *Int. Comm. Heat Mass Transfer*, 1988, **15**, 17.
4. Lai, F. C. and Kulacki, F. A., *Int. J. Heat Mass Transfer*, 1991, **34**, 1189.
5. Gebhart, B. and Pera, L., *Int. J. Heat Mass Transfer*, 1971, **14**, 2025.
6. Pera, L. and Gebhart, B., *Int. J. Heat Mass Transfer*, 1972, **15**, 269.
7. Radwan, A. E, and Elbashbeshy, E. M. A., *Il Nuovo Cimento*, 1990, **1053**, 615.
8. Chen, T. S. and Yuh, C. F., *Heat Transfer*, 1979, **2**, 233.
9. Lai, F. C., *Int. Comm. Heat Mass Transfer*, 1991, **18**, 93.
10. Yih, K. A., *Int. Comm Heat Mass Transfer*, 1997, **24**, 265.
11. Vajravelu, K. and Nayfeh, J., *Int. Comm. Heat Mass Transfer*, 1992, **19**, 701.
12. Chamkha, A. J., *Int. Comm. Heat Mass Transfer*, 1996, **23**, 875.
13. Vajravelu, K. and Hadjinicolaou, A., *Int. J. Eng. Sci.*, 1997, **35**, 1237.
14. Elbashbeshy, E. M. A., *Int. J. Eng. Sci.*, 1997, **34**, 515.
15. Blottner, F. G., *AIAA Journal*, 1970, **8**, 193.
16. Carnahan, B., Luther, H. A. and Wilkes, J. O., *Applied Numerical Methods*, 1969, John Wiley & Sons, Inc., New York, Chapter 7.